

pubs.acs.org/cm Article

# Leveraging Non-Covalent Interactions to Control the Morphology and Electrical and Mechanical Properties of Stretchable Semiconducting Composites

Yunfei Wang, Kai-Lin Chen, Angela Awada, Nathaniel Prine, Zhiqiang Cao, Chenhui Zhu, Yu-Cheng Chiu,\* Simon Rondeau-Gagné,\* and Xiaodan Gu\*



Cite This: https://doi.org/10.1021/acs.chemmater.3c02131



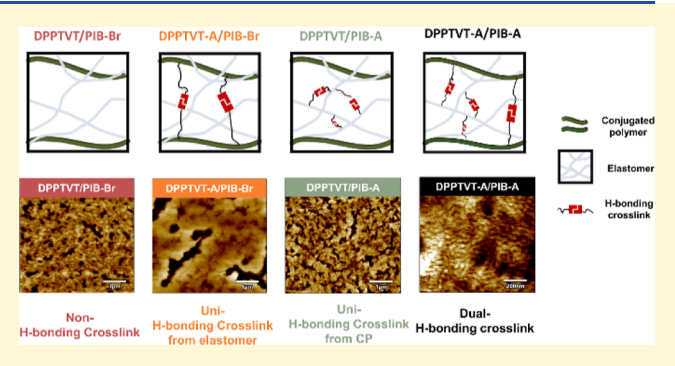
**ACCESS** I

III Metrics & More

Article Recommendations

Supporting Information

ABSTRACT: Physical blending conjugated polymers (CPs) with elastomers has been established as an effective method for enhancing the stretchability of semiconductors. However, predictable control of the morphology for incompatible polymer rubber blends remains a challenge. In this work, we demonstrated the control of phase separation size of CP/elastomer composites by strategically controlling the location sites of H-bonding functional groups in CPs and elastomers, while investigating their effects on mechanical and electrical properties. We incorporated amide functional groups into a DPP-based semiconducting polymer (DPPTVT-A) and polyisobutylene-based elastomer (PIB-A) to enable inter- and intraphase hydrogen bonding (H-bonding) cross-



links within CP/elastomer composites. Along with their nonamide counterparts, we fabricated four different CP/elastomer composites, DPPTVT-A/PIB-A, DPPTVT-A/PIB, DPPTVT/PIB-A, and DPPTVT/PIB, with dual-, uni-, and non-H-bonding cross-links and compared their phase behavior and electronic and mechanical properties. The location of the H-bonding greatly influenced the property of the semiconducting rubber as characterized by scattering, spectroscopy, and electrical characterization. Importantly, we found that creating a H-bonding cross-link into both domains of CP/elastomer composites can not only improve energy dissipation upon stretching but also maintain the electrical performance when applying high tensile stress. This work provides a comprehensive study of the morphology of CP/elastomer composites, offering valuable insights into the future design of stretchable CP/elastomer composites.

# ■ INTRODUCTION

Stretchable semiconductors play a crucial role in the development of wearable and implantable devices such as healthcare monitoring, flexible electronics, and smart textiles.<sup>1–8</sup> Conjugated polymers (CPs), known for their unique tunable organic structures through synthesis, hold significant potential as stretchable semiconductors compared to their inorganic counterparts.<sup>9–12</sup> However, the inherent rigidity and coplanarity of CPs' backbone, combined with their high degree of crystallinity-enhancing charge mobility, contradict the requirement for CPs to be soft and highly stretchable.<sup>13–15</sup> To address this challenge, researchers have explored various strategies to enhance stretchability. These strategies include the incorporation of long alkyl side chains, <sup>16–20</sup> the introduction of conjugation break spacers, <sup>15,21–27</sup> and the insertion of elastomer blocks.

Fabricating CP/elastomer composites through physical blending has emerged as a simple but highly efficient and promising strategy for developing stretchable semiconductors. In this approach, CPs are incorporated into an elastomer matrix, capitalizing on the soft and stretchable nature

of elastomers to impart high stretchability to the composites. More importantly, some of these composites have shown the ability to maintain or even improve charge mobilities. 42,43 Commonly used elastomers include polydimethylsiloxane (PDMS), 42,44-46 styrene—ethylene—butylene—styrene (SEBS), 34,37,38,47 polystyrene-block-polyisoprene-block-polystyrene (SIS), 48 and rubbers. 35,49 For example, the Reichmanis group blended poly(3-hexylthiophene-2,5-diyl) (P3HT) into PDMS, resulting in a significant improvement in stretchability from 5% to more than 100%, accompanied by an increased charge mobility of 0.052 to 0.11 cm<sup>2</sup>/V s. Later on, Zheng *et al.* incorporated covalent cross-links between azide and the C=C group in SEBS and the C-C bond in CPs, successfully

Received: August 22, 2023 Revised: October 25, 2023 Accepted: October 26, 2023



developing an elastic composite, DPPTT/SEBS, which did not show residual strain with increasing cyclic strain from 10 to 70%. Recently, Li et al. blended a redox-active semiconducting polymer with a bioadhesive brush polymer, successfully achieving rapid and strong adhesion with wet tissue surfaces. This material showcased high charge-carrier mobility of ~1 cm²/V s, high stretchability, and good biocompatibility, demonstrating great potential for in vivo bioadhesive organic electrochemical transistors measuring underskin electromyograms from the gastrocnemius medialis muscle. In our previous work, we blended DPP-T with a hydrogen bonding cross-linked elastomer PIB-amide, successfully achieving a crack onset strain (COS) of ~1500% while maintaining a charge mobility of 0.15 cm²/V s. 43

The morphology of CP/elastomer semiconducting composites was reported to have significant impacts on electrical and mechanical properties. S2,53 Nanofibril aggregates have been identified as a crucial factor in enhancing the charge mobility of CP/insulator composites, primarily due to the connectivity between these nanofibril aggregates. 47,52 For example, Angunawela et al. blended PDPP3T and polystyrene (PS) in various ratios.<sup>52</sup> With an increase in the PS ratio, the composites exhibited larger and more extended fibril networks, resulting in a higher charge mobility. Similarly, Nikzad et al. blended P2TDPP2TFT4 with SEBS, resulting in improved polymer aggregation and orientation, leading to a 5-fold increase in charge mobility from 0.3 to 1.5 cm<sup>2</sup>/V s.<sup>47</sup> Consequently, current research on stretchable semiconducting composites has made significant efforts to promote fiber-like aggregates. 38,54,55 In a very successful example, Xu et al. blended DPPT-TT into a SEBS matrix to utilize the nanoconfinement effect to induce the formation of fibril aggregates and successfully maintained a high charge mobility of 1 cm<sup>2</sup>/V s at 100% strain.<sup>38</sup> Additionally, the formation of bundle-like aggregations have proven beneficial for achieving mechanical stretchability.<sup>37</sup> Jeong et al. blended P3HT into PDMS, resulting in the formation of a P3HT bundle network, which significantly improved the stretchability with the COS exceeding 50%.<sup>37</sup> However, the careful manifestation of the morphology for stretchable CP/elastomer composites is still lacking, and further understanding of its influence on both mechanical and electrical properties remains to be investigated.

Introducing hydrogen bonding (H-bonding) cross-links into two incompatible polymers is an effective method to control the morphology of polymer composites. 56-58 For example, polystyrene/polyethylene glycol (PS/PEG) composites perform a large phase separation due to their inherent incompatibility. So After introducing complementary H-bonding into their chain ends, large phase separation was depressed, resulting in microphase separation. Similarly, when introducing ureidopyrimidinone (UPy) groups to a chain end of P3HT and PS to enable strong H-bonding interactions, large macroscale phase separations were successfully depressed. 60 The same phenomenon was also observed for poly(9,9-dioctyl fluorene) (PFO)/PEG and poly(3-hexylthiophene) (P3HT)/PFO composites. Therefore, H-bonding cross-links serve as an effective method for controlling the morphology of CP/elastomer composites. In addition, H-bonding cross-links can also improve stretchability. The relatively weak H-bond can be broken upon stretching, allowing for additional energy dissipation pathways to improve the stretchability of materials. Yan et al. introduced ureidopyrimidinone (UPy) groups to construct aH-bonding cross-linked supramolecular polymeric

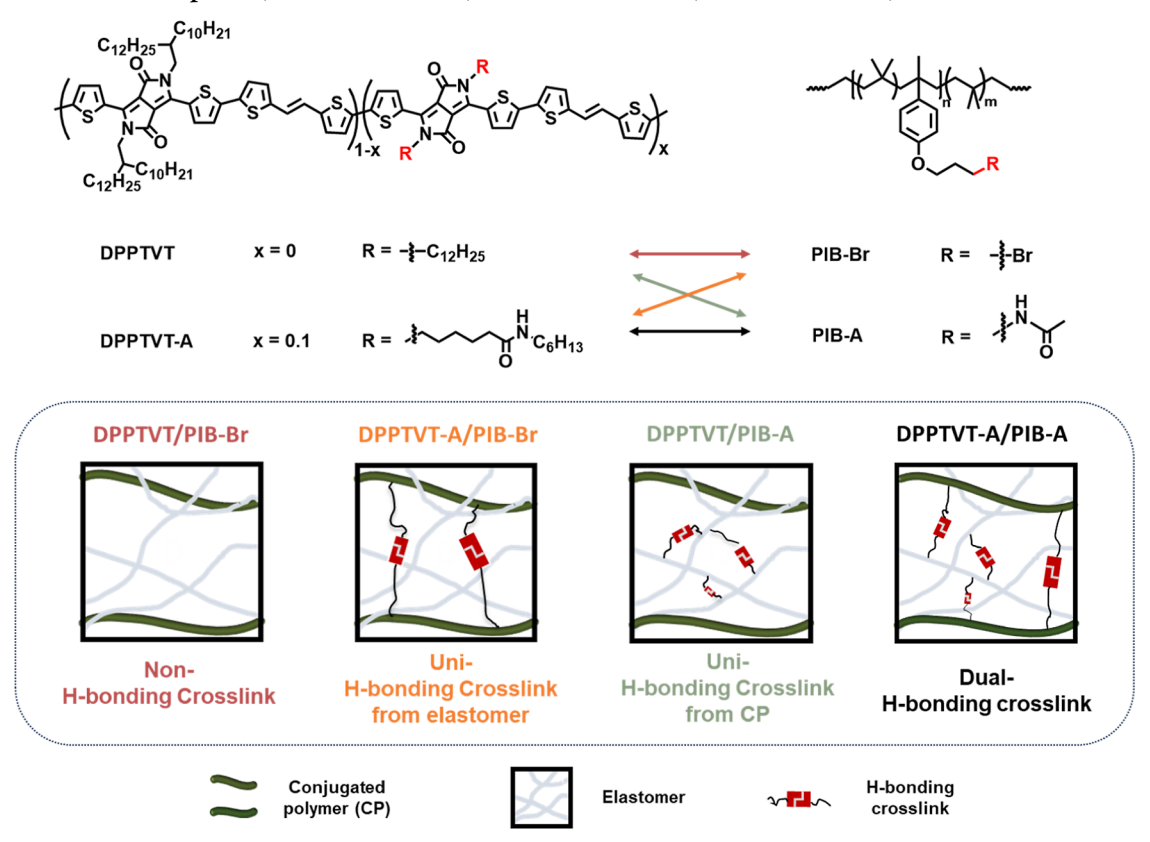
material.<sup>61</sup> With 20 mol % UPy groups incorporated, the supramolecular polymeric material achieved extreme stretchability (COS = 17,000%). Oh *et al.* introduced 2,6-pyridine dicarboxamide (PDCA) into DPP-based CP to enable a H-bonding cross-link between the CP backbones. The COS was effectively improved from 5% to over 100%.<sup>23</sup> Chen *et al.* introduced amide groups into soft phase polyacrylate and copolymerized with rigid PS.<sup>62</sup> With the H-bonding cross-link, the materials performed as a microphase-separated system, which enhanced toughness and self-healing ability. From these works and reporting, we hypothesize that introducing H-bonding cross-links into both CPs and elastomers can effectively control the morphology of CP/elastomer composites and modulate the mechanical and electrical properties.

In this work, we introduced amide functional groups to DPPTVT polymers to obtain a DPPTVT-A and PIB elastomer matrix (amide-polyisobutylene, PIB-A) respectively, allowing for formation of intra- and interphase H-bonding cross-links. By blending amide- or nonfunctional CPs and elastomers, four composites with different H-bonding cross-linking sites were fabricated: dual-H-bonding cross-linked DPPTVT-A/PIB-A, uni-HB cross-linked DPPTVT-A/PIB-Br, and DPPTVT/PIB-A and non-HB cross-linked DPPTVT/PIB-Br composites. Their morphologies were studied combining atomic force microscopy (AFM), atomic force microscopy with infrared spectroscopy (AFM-IR), grazing-incidence wide-angle X-ray scattering (GIWAXS), and UV-vis absorption spectroscopy. The mechanical properties were studied using a film-on-water and film-on-elastomer tensile tester. The effect on electrical properties was studied by fabricating top-contact bottom-gate organic field-effect transistors (OFETs). The non-H-bonding cross-linked composite exhibited the most pronounced fibril aggregation and highly ordered crystallite packing, resulting in the highest charge mobility but the lowest stretchability. Introducing intraphase H-bonding cross-links in CPs and elastomers led to larger and more large-scale aggregates due to stronger interactions, resulting in lower charge mobility but enhanced stretchability. Additionally, the charge mobility remained stable after stretching. Most interestingly, the dual-H-bonding cross-linked composite DPPTVT-A/PIB-A exhibited microphase separation due to a combination of interand intraphase H-bonding interactions. However, the microphase separation morphology was not beneficial to electrical properties, resulting in the lowest charge carrier mobility. After stretching, the two phases reorganized into fibrillike aggregates, obtaining improved charge mobility. In addition, from the polarized UV-vis spectroscopy study, the elastomer phaseprimarily contributed to the deformation for all the composites. The H-bonding introduced at the elastomer phase also improved the cyclic stretching stability, and both locations improved the self-healing abilities. This work provides a method to control the morphology of stretchable CP/ elastomer composites, enabling the complete understanding of morphological effects on mechanical and electrical properties, which will valuably guide the future design of stretchable semiconductors.

# **■ EXPERIMENTAL SECTION**

**Materials.** DPPTVT ( $M_{\rm n}=23.0~{\rm kDa}$ ), DPPTVT-A ( $M_{\rm n}=12.9~{\rm kDa}$ ), and PIB-Br ( $M_{\rm n}=56.1~{\rm kDa}$ ) and PIB-A ( $M_{\rm n}=56.1~{\rm kDa}$ ) were synthesized according to previous work. <sup>43,63,64</sup> Poly(sodium 4-styrenesulfonate solution) (PSS, 30% in water) was purchased from Sigma-Aldrich.

Scheme 1. Chemical Structures of DPPTVT, DPPTVT-A, PIB-Br, and PIB-A and Schematic of Non-, Uni- and Dual-H-Bonding Crosslinked Composites, DPPTVT/PIB-Br, DPPTVT-A/PIB-Br, DPPTVT/PIB-A, and DPPTVT-A/PIB-A



**Film Processing.** CPs, DPPTVT, and DPPTVT-A were blended with elastomers, PIB-Br and PIB-A, respectively, with a CP/elastomer weight blending ratio of 1:4 in anhydrous chlorobenzene at concentrations of 10 mg/mL. The solutions were heated at 80 °C overnight before processing. Thin films were spin-cast on Si wafers at 1000 rpm for 1 min. The thin-film thickness was  $\sim$ 60 nm. Thick films were drop-cast on precut Si wafers with a thickness of  $\sim$ 40  $\mu$ m.

Stretched thin films were first spin-cast on the OTS-treated  ${\rm Si/SiO_2}$  wafers and transferred to PDMS substrates. The thin films were stretched together with the PDMS substrate and transferred back onto Si wafers.

Atomic Force Microscopy and Infrared-Spectroscopy Combined AFM. AFM images were acquired on an Asylum Cypher S AFM microscope in AC-air mode. Composite thin films on Si wafers were observed.

AFM-IR was performed using nanoIR3 AFM-IR from Anasys Instruments (Santa Barbara, CA) coupled to a MIRcat-QT quantum cascade, mid-infrared laser (frequency range of 917–1700 and 1900–2230 cm<sup>-1</sup> and repetition rate of 1470 kHz). AFM-IR data was collected in tapping mode using a gold-coated AFM probe (spring constant [k]: 40 N m<sup>-1</sup> and resonant frequency  $[f_o]$ : 300 kHz). The pulsed mid-IR laser was tuned to resonance bands unique to each component, as determined by FTIR characterization (1666 cm<sup>-1</sup> for DPPTVT-A and 1462 cm<sup>-1</sup> for PIB-A). Acquired images were flattened using Analysis Studio software.

Grazing-Incidence Wide-Angle X-ray Scattering. GIWAXS measurements were conducted on beamline 7.3.3 at the Advanced Light Source in Berkeley Lawrence National Lab. Data was collected under a helium environment with an incident beam energy of 10 keV and an incidence angle of 0.14°. Composite thin-film samples were collected on Si wafers. The scattering signal was collected by a Pilatus 2M detector and processed using Igor 8 software combined with the Nika package and WAXSTools.

**UV-Vis Absorption Spectroscopy.** UV-vis-NIR spectra were acquired using a Cary 5000 UV-vis-NIR spectrophotometer.

Composite thin films were spin-cast on OTS-treated Si/SiO $_2$  wafers and transferred to the PDMS substrates. Polarized UV—vis spectroscopy was recorded using polarized light with angles of 0 and 90° to the strain direction.

**Film-on-Elastomer Tensile Test.** Composite thin films were first spin-cast on the OTS-treated  $Si/SiO_2$  wafers and transferred to PDMS substrates. The thin films were stretched together with the PDMS substrate using a manual linear stage. The images were taken at the engineering strain of 0, 20, 50, 100, 150, and 200% using optical microscopy (Zeiss Axio Imager).

**Film-on-Water Tensile Test.** Tensile tests of composites were performed by using thick films. The films were prepared on PSS-coated Si wafers followed by being floated on top of water and stretched at a strain rate 2 s<sup>-1</sup> until fracture. The detailed instrument setup can be found in previous literature reports. <sup>65,66</sup>

**OFET Fabrication and Characterization.** The device performance for stretched composites was measured under a strain-neutral state. To prepare the samples, 80 nm thin films were spin-coated on OTS-treated Si/SiO<sub>2</sub> wafers and transferred to PDMS substrates. The thin film was uniaxially stretched on PDMS and transferred fresh to Si wafers. Finally, gold electrodes were deposited to obtain top-contact bottom-gate OFETs. The error bars were associated with multiple devices with the same fabrication method.

## ■ RESULTS AND DISCUSSION

The overall design strategy of semiconducting composites with or without H-bonding is shown in Scheme 1. We aim to control the morphology of stretchable CP/elastomer composites by introducing H-bonding cross-links at different sites (no interaction or with intra- or interphase H-bonding cross-links) and study the following effect on mechanical and electrical properties. Amide functional DPPTVT (DPPTVT-A) and amide functional PIB (PIB-A) were synthesized to endow the capability to form H-bonding cross-linking networks. <sup>43,63</sup> Their

Table 1. Summary of Morphological, Electrical, and Mechanical Properties of Non-, Uni-, and Dual-H-Bonding Crosslinked Composites, DPPTVT/PIB-Br, DPPTVT-A/PIB-Br, DPPTVT/PIB-A, and DPPTVT-A/PIB-A

sample	morphology					electrical property		
	AFM GIW		polarized UV– VAXS vis spectroscopy		COS (%)	$\begin{array}{ll} \text{charge} \\ \text{mobility} & \text{charge mobility up} \\ \text{(cm}^2/\text{V s)} & \text{stretching (cm}^2/\text{V} \end{array}$		
		lamellar peak (Å <sup>-1</sup> )	lamellar peak fwhm (Å <sup>-1</sup> )	0-0/0-1 peak intensity ratio			ε = 50%	ε = 150%
DPPTVT/ PIB-Br	dominated fiber aggregates, large-scale aggregates	0.30	0.05	1.04	<100	$0.45 \pm 0.05$	$0.46 \pm 0.03$	$0.17 \pm 0.01$
DPPTVT- A/PIB-Br	reduced fiber aggregates, larger large-scale aggregates	0.27	0.11	1.18	100-150	$0.16 \pm 0.02$	$0.18 \pm 0.02$	$0.16 \pm 0.02$
DPPTVT/ PIB-A	reduced fiber aggregates, more large-scale aggregates	0.30	0.05	1.02	>200	$0.08 \pm 0.01$	$0.05 \pm 0.01$	$0.09 \pm 0.01$
DPPTVT- A/PIB-A	microphase separation, large- scale aggregates	0.27	0.08	1.19	>200	$0.02 \pm 0.01$	$0.04 \pm 0.01$	$0.06 \pm 0.01$

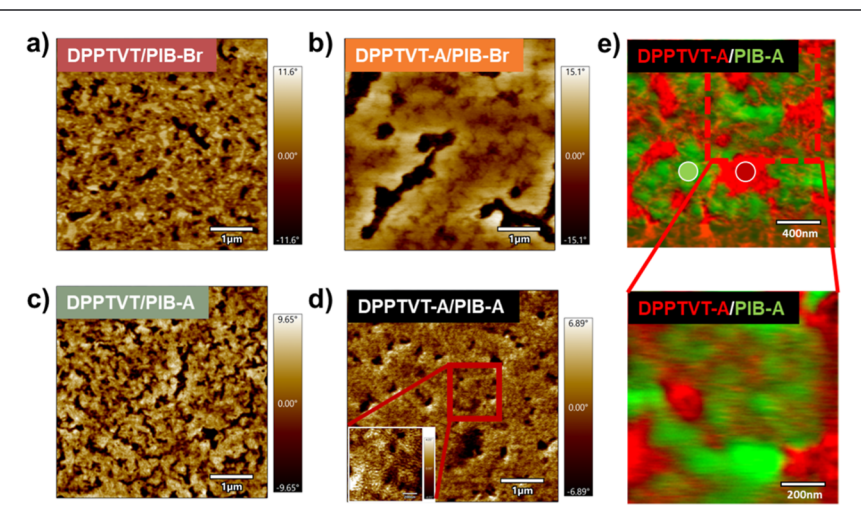


**Figure 1.** AFM phase images of (a) DPPTVT/PIB-Br, (b) DPPTVT-A/PIB-Br, and (c) DPPTVT/PIB-A and (d) DPPTVT-A/PIB-A composites. (e) AFM-IR overlay image highlighting the distributions of DPPTVT-A and PIB-A in DPPTVT-A/PIB-A composite films (red color represents DPPTVT-A domains selectively excited using a 1666 cm<sup>-1</sup> laser, and the green color represents PIB-A domains selectively excited using a 1462 cm<sup>-1</sup> laser).

nonamide counterparts DPPTVT and PIB-Br were used as the non-H-bonding cross-linked control sample. By blending DPPTVT-A and DPPTVT with PIB-A and PIB-Br, four CP/ elastomer composites with different H-bonding cross-linked sites were fabricated including dual-H-bonding cross-linked composite, DPPTVT-A/PIB-A, with both inter- and intraphase H-bonding cross-links, uni-H-bonding cross-linked composites, DPPTVT-A/PIB and DPPTVT/PIB-A, with intra-CP or intraelastomer H-bonding cross-link, and non-H-bonding cross-linked composite, DPPTVT/PIB-Br. All the composites used a CP/elastomer 1:4 weight ratio, which was the optimized ratio in terms of mechanical and electrical properties reported in previous studies. 43 Fourier-transform infrared (FT-IR) spectroscopy was used to confirm the formation of H-bonding cross-links, primarily by analyzing the wide -NH stretching peak in the range of 3700-3100 cm<sup>-1</sup> (Figure S1a).<sup>6</sup> However, the presence of an overlapping peak from the elastomer phase (Figure S1b) and the shared utilization of amide groups for H-bonding cross-link formation in both components made it impossible to differentiate the location of these cross-links. We expected the H-bonding cross-linking to effectively reduce phase separation between the semiconducting polymer and elastomer phase and have an influence on the electrical and mechanical properties (Table 1).

The morphology of composites was first characterized by AFM, GIWAXS, and UV-vis spectroscopy. AFM was employed to determine the surface morphology of the composites. The non-H-bonding cross-linked composite, DPPTVT/PIB-Br, exhibited predominated large fibril aggregates, which was commonly observed in CP/elastomer composites in literature (Figures 1a and S2a). Upon the introduction of H-bonding cross-links into CPs, the number of fibril aggregates decreased, while the size of large-scale aggregates increased obviously (Figures 1b and S2b). This observation can be attributed to stronger fibril aggregates induced by the additional H-bonding interaction between CP chains. Conversely, when H-bonding cross-links were introduced within the elastomer phase, the size of large-scale aggregates from DPPTVT CPs remained constant, similar to the non-H-bonding cross-linked composite DPPTVT/PIB-Br, while their quantity increased (Figures 1c and S2c). Thus, the constant size of aggregates resulted from the consistent interaction strength between CPs. However, the H-bonding cross-links within the elastomer phase led to a preference of more large-scale aggregates formed from fibril aggregates. Consequently, in uni-H-bonding cross-linked composites, the H-bonding cross-links within CPs dominated the size of the large-scale aggregates, while the H-bonding cross-links within

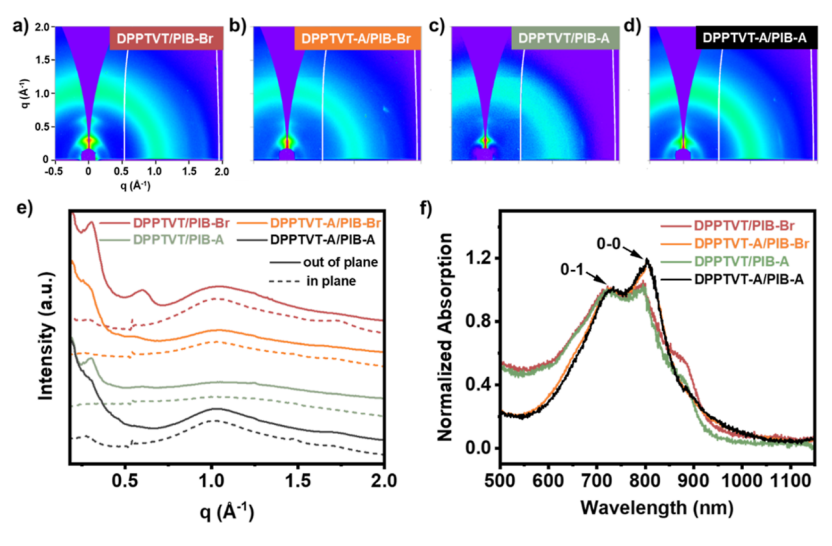


Figure 2. GIWAXS and UV—vis results of composites. 2D images for (a) DPPTVT/PIB-Br, (b) DPPTVT-A/PIB-Br, (c) DPPTVT/PIB-A, and (d) DPPTVT-A/PIB-A composites from GIWAXS. (e) 1D line-cut profiles for DPPTVT/PIB-Br (red), DPPTVT-A/PIB-Br (orange), DPPTVT/PIB-A (green), and DPPTVT-A/PIB-A (black) composites in both out-of-plane direction (solid line) and in-plane direction (dotted line) from GIWAXS. (f) UV—vis absorption spectra of DPPTVT/PIB-Br (red), DPPTVT-A/PIB-Br (orange), DPPTVT/PIB-A (green), and DPPTVT-A/PIB-A (black) composites.

Table 2. Crystallographic Parameters of Non-, Uni-, and Dual-H-Bonding Crosslinked Composites, DPPTVT/PIB-Br, DPPTVT-A/PIB-Br, DPPTVT/PIB-A, and DPPTVT-A/PIB-A from GIWAXS

materials		out of plane		in plane			
	lamellar peak (Å <sup>-1</sup> )	lamellar peak FWHM (Å <sup>-1</sup> )	$\pi$ - $\pi$ stacking (Å <sup>-1</sup> )	lamellar peak (Å <sup>-1</sup> )	lamellar peak FWHM (Å <sup>-1</sup> )	$\pi$ - $\pi$ stacking $(\mathring{A}^{-1})$	
DPPTVT/PIB-Br	0.30	0.05	/	0.29	0.05	1.73	
DPPTVT-A/PIB-Br	/	/	/	0.27	0.11	/	
DPPTVT/PIB-A	0.30	0.05	/	/	/	/	
DPPTVT-A/PIB-A	/	/	/	0.27	0.08	/	

the elastomer dominated the number of large-scale aggregates. Interestingly, a microphase separation morphology emerged in the dual-H-bonding cross-linked composite DPPTVT-A/PIB-A, accompanied by the presence of large-scale aggregates (Figures 1d,e and S2d,e), originating from the interphase Hbonding cross-link between the elastomer and CP chains. To further confirm the microphase separation morphology, AFM-IR was employed to highlight the distribution of the DPPTVT-A/PIB-A composite (Figure 1e). We selectively excited the DPPTVT-A and PIB-A phase using a 1666 cm<sup>-1</sup> laser and a 1462 cm<sup>-1</sup> laser, respectively. Those two wavelengths were selected from the unique absorption spectrum shown in Figure S3. The red color represents the DPPTVT-A domain, while the green color represents the PIB-A domain. A similar result was observed, showing microphase separation, further supporting the presence of microphase separation. The bottom surface morphology for the composites was also assessed using AFM due to its relevance to charge mobility. The composite films were initially spin-cast onto OTS-treated Si/SiO2 wafers and subsequently transferred onto PDMS. AFM imaging of the bottom surface was conducted using PDMS as substrates. Remarkably, all the four composites exhibited a similar morphology (Figure S4). We attributed this similarity to the comparable surface energy of these composites when compared to the Si wafer surface. It is worth noting that due to the thinness of the composite films, variations in morphology between the top and bottom surfaces have little impact on their electronical properties.

GIWAXS and UV-vis were then employed to investigate the crystalline structure and aggregation behavior of the CP domain in the composites. The 2D scattering patterns and corresponding 1D scattering profiles from GIWAXS are shown in Figure 2a—e. The fitting peak position and full width at halfmaximum (FWHM) of the lamellar packing (100) and  $\pi - \pi$ stacking (010) are summarized in Table 2. It should be noted that some peaks could not be fitted due to the weak scattering signal resulting from the disordered nature of CPs in the composites. Lamellar packing peaks were observed for all composites, indicating the formation of a crystalline structure for the CP phase for all composites. The non-H-bonding crosslinked composite DPPTVT/PIB-Br exhibits the most prominent higher-order lamellar packing peak (200), indicating the most ordered crystalline packing among the composites. In the uni-H-bonding cross-linked composites, DPPTVT-A/PIB-Br and DPPTVT/PIB-A, a weaker (200) peak was observed, suggesting a less ordered crystalline packing. In the dual-Hbonding cross-linked composite, DPPTVT-A/PIB-A, only a weak (100) peak was observed, with no clear (200) peak visible, indicating a nearly amorphous structure. This amorphous structure is likely a result of the interphase Hbonding cross-links, which hinder the formation of crystalline structure in the DPPTVT-A/PIB-A composite. Additionally, composites with the same CP compounds exhibited similar lamellar packing distance, with values of 20.9 Å for DPPTVT/ PIB-Br and DPPTVT/PIB-A composites and 23.3 Å for DPPTVT-A/PIB-Br and DPPTVT-A/PIB-A composites, in-

dicating that the lamella packing distance is side chain-dependent for these CPs. The (010) peak of non-H-bonding cross-linked composite DPPTVT/PIB-Br appeared in the inplane direction, suggesting a predominantly edge-on orientation. In contrast, no (010) peak was observed in the other three composites, further confirming the presence of a less-ordered crystalline structure.

UV—vis absorption spectroscopy was utilized to investigate the aggregation behavior of CP chains in the composites (Figure 2f). The 0–0 and 0–1 peaks were observed in all composites, indicating the presence of CP aggregations in all composites, which is consistent with the morphology observed in AFM. All of the curves were normalized with the 0–1 peak. The composites containing DPPTVT-A exhibited stronger 0–0 peaks compared to the composites containing DPPTVT, which can be attributed to the additional H-bonding cross-links between CP phases.

The effect of morphology on device performance was then investigated by fabricating top-contact bottom-gate OFETs as shown in Figures 3 and S5. The non-H-bonding cross-linked

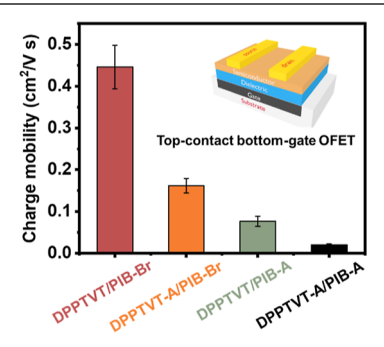


**Figure 3.** Charge mobility comparison of DPPTVT/PIB-Br (red), DPPTVT-A/PIB-Br (orange), DPPTVT/PIB-A (green), and DPPTVT-A/PIB-A (black) composites.

composite, PIB-Br/DPPTVT, exhibited the highest charge mobility, 0.45 cm<sup>2</sup>/V s. This excellent device performance was attributed to the predominated fibril aggregation and the highest ordered crystalline packing, as discussed previously. However, when H-bonding cross-links were introduced into CPs, the mobility decreased to 0.16 cm<sup>2</sup>/V s due to the reduction of fibril aggregates and less-order crystalline packing. Furthermore, when H-bonding cross-links were introduced into the elastomer phase, the charge mobility further decreased to 0.08 cm<sup>2</sup>/V s, primarily due to the further decreased amounts of fibril aggregates. Surprisingly, when both components were cross-linked with H-bonds, the DPPTVT-A/PIB-A composite exhibited the lowest mobility, 0.02 cm<sup>2</sup>/V s, which can be attributed to the minimal fibril aggregates and nearly amorphous structure. The hysteresis of the composites was also analyzed from the transfer curves (Figure S5). The PIB-A/DPPTVT-A composite showed remarkable hysteresis due to the doping of electrons by the amide groups in both components.

The mechanical properties of the composites were next studied by using film-on-elastomer and film-on-water tensile tests. Considering the H-bonding cross-linking influence on mechanical properties, the results originate from an association effect of morphology and H-bonding cross-links. Film-on-elastomer tensile tests were performed to evaluate the stretchability of the composite thin films. The spin-cast

composite thin films were transferred to PDMS and stretched to fixed strains. Optical microscopic (OM) images were used to monitor the formation of cracks (Figures 4a and S6). Due to the limitation of PDMS, we only stretched them to a strain of 200%. At 200% strain, only the DPPTVT/PIB-Br composite showed noticeable cracks. AFM images of stretched composites were also obtained in the following study, which revealed smaller cracks. The DPPTVT/PIB-Br composite exhibited cracks starting at a strain of 100%, while the DPPTVT-A/PIB-Br composite showed cracks at a strain of 150%, indicating that the COS of the DPPTVT/PIB-Br composite was less than 100% and the COS of DPPTVT-A/ PIB-Br was between 100 and 150% (Figure 6a). In contrast, the other composites exhibited a COS higher than 200%. These results indicate that introducing H-bonding cross-links to CP phases slightly improved stretchability, while introducing H-bonding cross-links to elastomer phases significantly enhances the stretchability. A film-on-water tensile test was conducted to study the modulus of the composites (Figures 4b and S7). Thick films with  $\sim$ 40  $\mu$ m thickness were drop-cast on polystyrenesulfonate salt spin-cast Si wafers and transferred onto a water surface. The representative stress-strain curves are shown in Figure 4b, and the elastic modulus (E) extracted from the slope of elastic region is summarized in Figure 4c. The non-H-bonding cross-linked composite, DPPTVT/PIB-Br, showed the lowest elastic modulus. After introducing Hbonding cross-links into the CP phase, the elastic modulus increased due to the physical cross-links between CP chains. When introducing H-bonding cross-links into the elastomer phase, the elastic modulus further increased. That is because the elastomer matrix dominates the mechanical properties of the composites. The H-bonding cross-links between elastomers showed a more straightforward influence on the modulus improvement than that between CPs. Interestingly, when Hbonding cross-links were introducing into both components, the E decreased slightly compared to the elastomer crosslinked composite, DPPTVT/PIB-A, which can be attributed to some of the amide groups in elastomers interacting with the CP chains, reducing the cross-link density of elastomers and lowering the E of the overall composites. Besides, the lower crystallinity observed from GIWAXS should also contribute to lowering the E. The COS determined from the film-on-water tensile test was observed to be lower than that from the filmon-elastomer tensile test, likely due to the presence of more aggregates formed during drop-casting, which act as defects in the films.

The charge mobility of stretched composites was also studied to evaluate the stretchability of composite films (Figures 5 and S8–S11). The sample preparation method was the same as that previously reported in the literature. Mobility measurements were conducted both parallel and perpendicular to the stretching direction. The mobility of the non-H-bonding cross-linked composite, DPPTVT/PIB-Br, started to decrease at a strain of 100% in both directions (Figure 5a). After introducing H-bonding cross-links into either the CP or elastomer phase, the charge mobility remained stable even after stretching to a strain of 150% (Figure 5b,c). For dual-H-bonding cross-linked DPPTVT-A/PIB-A, the mobility was first constant at an initial strain of 20% followed by a surprising increase at the strains of 50, 100, and 150% (Figure 5d).

To thoroughly comprehend the electrical property of the stretched composites, we conducted morphology analyses of

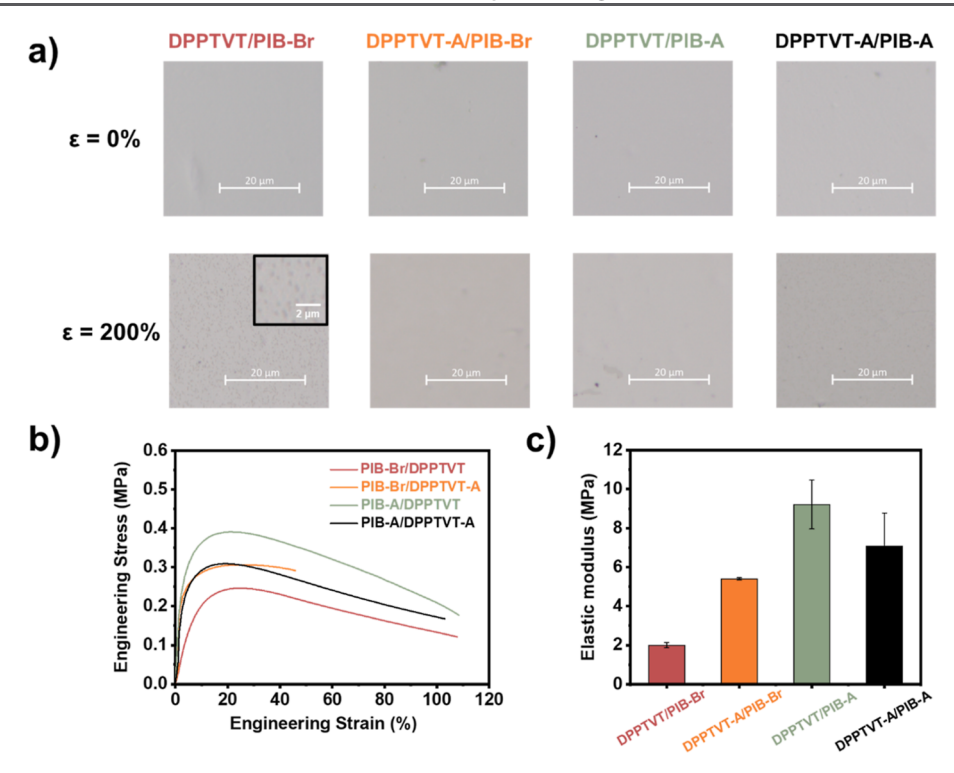


**Figure 4.** Mechanical properties of composites. (a) Representative optical images of the stretched composites strained *via* the film-on-elastomer tensile test. (b) Representative stress—strain curve and (c) elastic modulus of DPPTVT/PIB-Br (red), DPPTVT-A/PIB-Br (orange), DPPTVT/PIB-A (green), and DPPTVT-A/PIB-A (black) composites strained *via* the film-on-water tensile test.

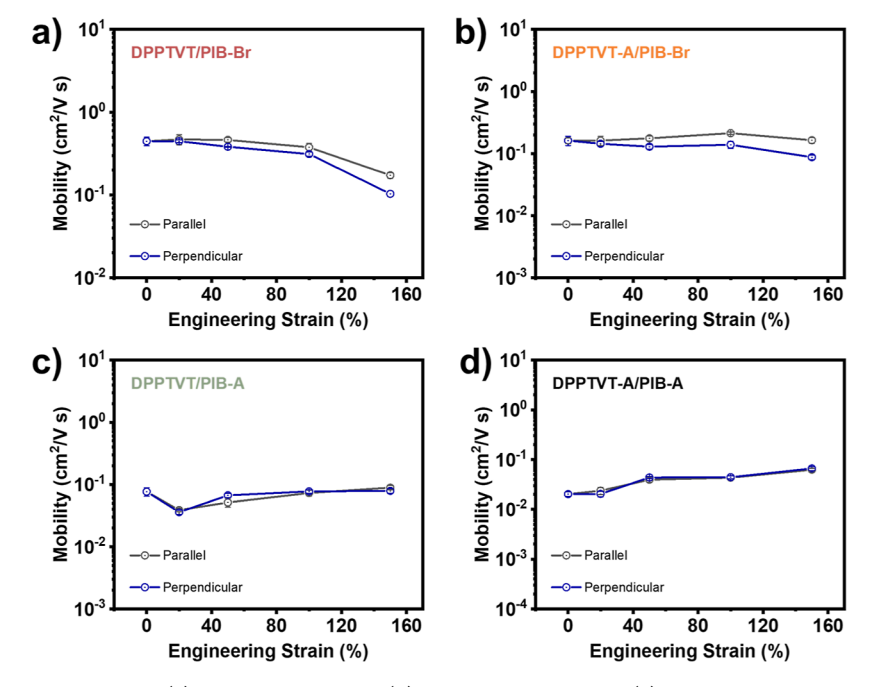


Figure 5. Charge mobility of stretched (a) DPPTVT/PIB-Br, (b) DPPTVT-A/PIB-Br, (c) DPPTVT/PIB-A, and (d) DPPTVT-A/PIB-A composites in parallel and perpendicular directions to the stretching direction at the engineering strains of 0, 20, 50, 100, and 150%, respectively.

stretched composites using AFM and polarized UV—vis spectroscopy. AFM was employed to investigate changes in surface morphology after stretching at different strains (Figures 6 and S12). For the non-H-bonding cross-linked composite DPPTVT/PIB-Br, the voids became larger at the strain of 50%, and cracks began to appear at the strain of 100%. This breakage explains the dropped charge mobility of the DPPTVT/PIB-Br composite at a strain of 100%. In contrast,

the morphologies of both uni-H-bonding cross-linked composites, DPPTVT-A/PIB-Br and DPPTVT/PIB-A, remained stable after stretching to 100%, resulting in stable charge mobility upon stretching. After stretching to 150%, intra-CP phase cross-linked composite DPPTVT-A/PIB-Br exhibited some cracks, leading to a decreased charge mobility. However, the intraelastomer cross-linked composite DPPTVT/PIB-A maintained its morphology even after being

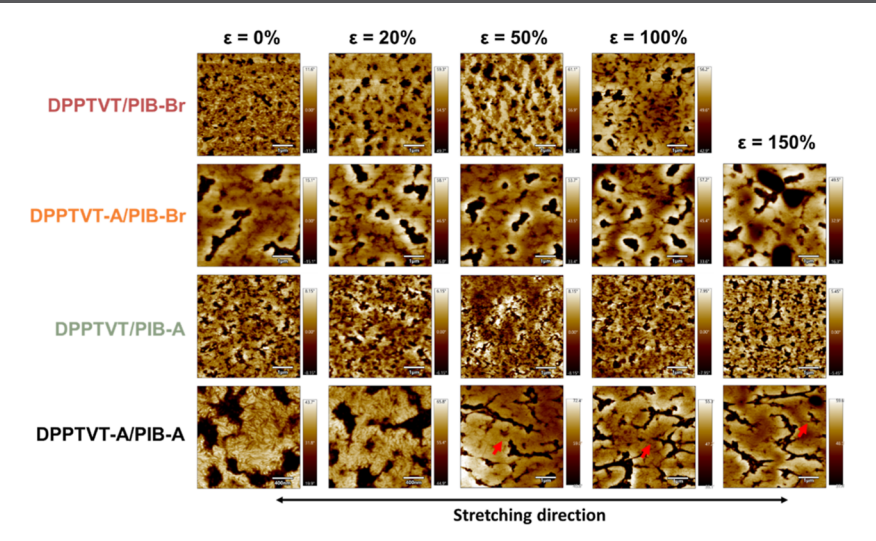
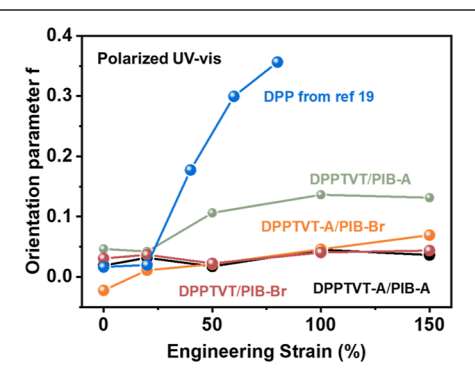


Figure 6. AFM phase images of stretched DPPTVT/PIB-Br (red), DPPTVT-A/PIB-Br (orange), DPPTVT/PIB-A (green), and DPPTVT-A/PIB-A (black) composites at strains of 0, 20, 50, 100, and 150%. The red arrows point out the fibril aggregates.

stretched to 150%, obtaining a stable charge mobility. For the dual-H-bonding cross-linked composite DPPTVT-A/PIB-A, the morphology remained unchanged after stretching to 20%, resulting in constant mobility at a strain of 20%. However, after stretching to a strain of 50%, the two phases reorganized and formed fibril aggregates, improving the charge mobility along both directions. These fibril aggregates remained stable after further stretching to 150%, resulting in maintained charge mobility. Polarized UV—vis spectroscopy was conducted to investigate the alignment of the whole CP chain for stretched DPPTVT/PIB-Br, DPPTVT-A/PIB-Br, DPPTVT/PIB-A, and DPPTVT-A/PIB-A composites at various strains (Figures 7



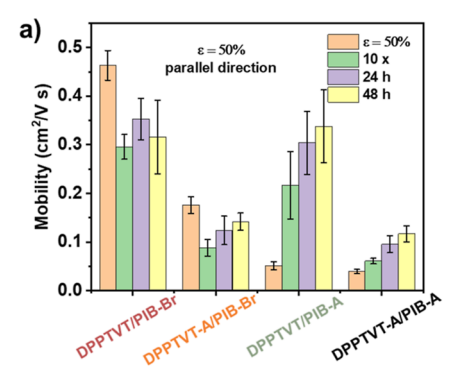
**Figure 7.** Herman's orientation parameter *f versus* engineering strain based on polarized UV—vis for DPPTVT/PIB-Br, DPPTVT-A/PIB-Br, DPPTVT/PIB-A, and DPPTVT-A/PIB-A composite films at 0, 20, 50, 100, and 150% strains.

and S13). The normalized absorption spectrum for the composite films under strains of 0, 20, 50, 100, and 150% is plotted in Figure S13. Peaks at  $\approx$ 795, 806, 800, and 804 cm<sup>-1</sup> correspond to the 0  $\rightarrow$  0 peaks of DPPTVT/PIB-Br, DPPTVT-A/PIB-Br, DPPTVT-A/PIB-A, and DPPTVT-A/PIB-A composites, respectively, while peaks at  $\approx$ 795, 806, 800, and 804 cm<sup>-1</sup> represent 0  $\rightarrow$  1 peaks. Orientation parameter f was calculated from the dichroic ratio, R, using the formula f = (R-1)/(R+1). For all the composites, f showed only a slight increase at a strain of 150% (0.09, 0.01, 0.09, and 0.02 for DPPTVT/PIB-Br, DPPTVT-A/PIB-Br, DPPTVT/PIB-A, and DPPTVT-A/PIB-A composites, respectively). These values

were significantly lower than the reported value for the pure DPP polymer (f = 0.36 at 100% strain), indicating that the whole chain of CPs did not align extensively. Combining these results with the AFM findings, it is evident that the deformation was primarily contributed by the elastomer phase in DPPTVT/PIB-Br, DPPTVT-A/PIB-Br, and DPPTVT/PIB-A composites, which is consistent with our previous report. In the case of DPPTVT-A/PIB-A composites, while the CP phase reorganized into fibrils after a strain of 50%, no distinct preferred orientation was observed.

The cyclic stretching stability and self-healing ability were evaluated by measuring the electrical performance after subjecting the composites to 10 cycles of stretching at strains of 50 and 150%, with subsequent rests of 24 and 48 h (Figures 8 and S14). Upon subjecting the composites to 10 cycles of stretching at a 50% strain, the charge mobility decreased for DPPTVT/PIB-Br and DPPTVT-A/PIB-Br composites. Conversely, the charge mobility increased for DPPTVT/PIB-A and DPPTVT-A/PIB-A composites, indicating that the introduction of H-bonding cross-links in the elastomer phase improves device stability during cyclic stretching at a 50% strain. However, after undergoing 10 cycles of stretching at a 150% strain, no consistent trend was observed among the composites. The charge mobility improved for DPPTVT/ PIB-Br and DPPTVT/PIB-A composites, decreased for DPPTVT-A/PIB-Br composites, and remained constant for DPPTVT-A/PIB-A composites. This suggests that H-bonding cross-links may not provide sufficient stability at very high strains (150%) for a non-chemically cross-linked network. Hysteresis changes after cyclic stretching were evaluated based on the transfer curves (Figure S15). At 50% strain, the hysteresis decreased after cyclic stretching for DPPTVT/PIB-Br and DPPTVT-A/PIB-Br, while there was almost no change for the DPPTVT/PIB-A and DPPTVT-A/PIB-A composites. This further confirms the enhanced device stability when introducing H-bonding cross-links in the elastomer phase. However, at a 150% strain, all hysteresis values remained unchanged after cyclic stretching, reinforcing that H-bonding cross-links may not significantly improve stability at higher strains.

To assess the self-healing ability of the composites, charge mobilities of the cyclic stretched composites were measured



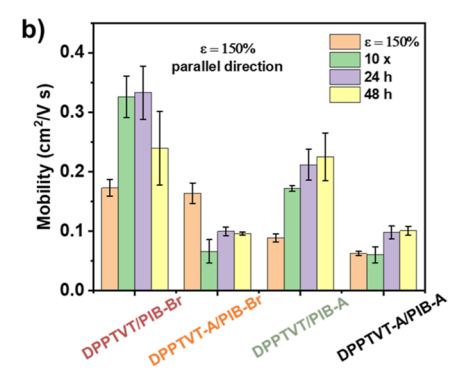


Figure 8. Charge mobility comparison along the parallel direction of DPPTVT/PIB-Br (red), DPPTVT-A/PIB-Br (orange), DPPTVT/PIB-A (green), and DPPTVT-A/PIB-A (black) composites after stretching 1 and 10 cycles and staying for 24 and 48 h at strains of (a) 50 and (b) 150%.

after 24 and 48 h (Figure 8 and S14). The charge mobility increased for DPPTVT-A/PIB-Br, DPPTVT/PIB-A, and DPPTVT-A/PIB-A composites after both 24 and 48 h, whereas it remained almost constant for DPPTVT/PIB-Br. This indicates that the introduction of H-bonding cross-links at either location enhances the self-healing ability, particularly when H-bonding is introduced into the elastomer phase, leading to charge mobility exceeding that of the original stretched state.

# CONCLUSIONS

In summary, we utilized the amide-functional CP and elastomer, DPPTVT-A and PIB-A, respectively, for formation of H-bonding cross-links to control the morphology of CP/ elastomer composites and further influence on mechanical and electrical properties. By blending amide- and nonamidefunctionalized CP and elastomers, we fabricated four different CP/elastomer composites including non-H-bonding crosslinked composite, DPPTVT/PIB-Br, uni-H-bonding crosslinked composites, DPPTVT-A/PIB-Br and DPPTVT/PIB-A, and dual H-bonding cross-linked composite, DPPTVT-A/PIB-A. The non-H-bonding composites exhibited predominant fibril aggregates and the highest degree of ordered crystalline structures, resulting in the highest charge mobility. However, these composites exhibited the poorest stretchability with the lowest COS and decreased mobility upon stretching. Introducing H-bonding cross-links in the CP or elastomer led to the larger and more large-scale aggregates, respectively, resulting in decreased charge mobility. However, the stretchability was improved, and the mobility was maintained after stretching. Most interestingly, the dual-H-bonding crosslinked composite, DPPTVT-A/PIB-A, displayed the lowest charge mobility, which could be attributed to the formation of microphase separation and large-scale aggregation without fibril formation. However, upon stretching, the H-bonds broke, and the two-phase reorganized into fibril aggregates, leading to an improvement in charge mobility. Importantly, it was found that creating H-bonding cross-links into both domains of CP/ elastomer composites not only improved stretchability but also maintained the electrical performance when applying high tensile stress. Besides, the H-bonding introduced at the elastomer phase also improved the cyclic stretching stability, and both locations will improve the self-healing ability. These findings shed light on controlling the morphology of CP/ elastomer composites and studying the effects of morphology on mechanical and electrical properties, which provides guidance in future designs of stretchable semiconductors.

#### ASSOCIATED CONTENT

# Supporting Information

The Supporting Information is available free of charge at https://pubs.acs.org/doi/10.1021/acs.chemmater.3c02131.

FT-IR spectroscopy; AFM height images; transfer curve; OM images; repeated stress—strain curves; UV-vis absorption spectroscopy; and charge mobility comparison in the perpendicular direction (PDF)

#### AUTHOR INFORMATION

# **Corresponding Authors**

Yu-Cheng Chiu — Department of Chemical Engineering, National Taiwan University of Science and Technology, Taipei 106, Taiwan; ⊚ orcid.org/0000-0003-4812-5681; Email: ycchiu@mail.ntust.edu.tw

Simon Rondeau-Gagné — Department of Chemistry and Biochemistry, Advanced Materials Centre of Research, University of Windsor, Windsor, Ontario N9B3P4, Canada; orcid.org/0000-0003-0487-1092;

Email: simon.rondeau-gagne@uwindsor.ca

Xiaodan Gu — School of Polymer Science and Engineering, Center for Optoelectronic Materials and Devices, The University of Southern Mississippi, Hattiesburg, Mississippi 39406, United States; orcid.org/0000-0002-1123-3673; Email: xiaodan.gu@usm.edu

## **Authors**

ı

Yunfei Wang — School of Polymer Science and Engineering, Center for Optoelectronic Materials and Devices, The University of Southern Mississippi, Hattiesburg, Mississippi 39406, United States; Oorcid.org/0000-0001-7555-5308

Kai-Lin Chen – Department of Chemical Engineering, National Taiwan University of Science and Technology, Taipei 106, Taiwan

Angela Awada – Department of Chemistry and Biochemistry, Advanced Materials Centre of Research, University of Windsor, Windsor, Ontario N9B3P4, Canada

Nathaniel Prine — School of Polymer Science and Engineering, Center for Optoelectronic Materials and Devices, The University of Southern Mississippi, Hattiesburg, Mississippi 39406, United States

Zhiqiang Cao — School of Polymer Science and Engineering, Center for Optoelectronic Materials and Devices, The University of Southern Mississippi, Hattiesburg, Mississippi 39406, United States

Chenhui Zhu – Advanced Light Source, Lawrence Berkeley National Laboratory, Berkeley, California 94720, United States

Complete contact information is available at: https://pubs.acs.org/10.1021/acs.chemmater.3c02131

#### **Notes**

The authors declare no competing financial interest. Published as part of *Chemistry of Materials*virtual special issue"In Honor of Prof. Elsa Reichmanis".

#### ACKNOWLEDGMENTS

We thank the National Science Foundation under award number DMR-2047689 for supporting this work. S.R.-G. thanks the Natural Sciences and Engineering Research Council of Canada (NSERC) for financial support through a Discover Grant (RGPIN-2022-04428). A.A. thanks the Government of Ontario for financial support through an Ontario Graduate Scholarship. K.-L.C. and Y.-C.C. thank the financial support from the Ministry of Science and Technology in Taiwan (MOST 111-2628-E-011-008-MY3). Work at the Molecular Foundry was supported by the Office of Science, Office of Basic Energy Sciences, of the U.S. Department of Energy under contract no. DE-AC02-05CH11231. This research used beamline 7.3.3 of the Advanced Light Source, which is a DOE Office of Science User Facility under contract no. DE-AC02-05CH11231. Y.W. was supported in part by an ALS Doctoral Fellowship in Residence.

## REFERENCES

- (1) Kim, D. H.; Lu, N.; Ma, R.; Kim, Y. S.; Kim, R. H.; Wang, S.; Wu, J.; Won, S. M.; Tao, H.; Islam, A.; Yu, K. J.; Kim, T. I.; Chowdhury, R.; Ying, M.; Xu, L.; Li, M.; Chung, H. J.; Keum, H.; McCormick, M.; Liu, P.; Zhang, Y. W.; Omenetto, F. G.; Huang, Y.; Coleman, T.; Rogers, J. A. Epidermal Electronics. *Science* **2011**, 333 (6044), 838–843.
- (2) Lipomi, D. J.; Bao, Z. Stretchable and Ultraflexible Organic Electronics. MRS Bull. 2017, 42 (02), 93–97.
- (3) Son, D.; Lee, J.; Qiao, S.; Ghaffari, R.; Kim, J.; Lee, J. E.; Song, C.; Kim, S. J.; Lee, D. J.; Jun, S. W.; Yang, S.; Park, M.; Shin, J.; Do, K.; Lee, M.; Kang, K.; Hwang, C. S.; Lu, N.; Hyeon, T.; Kim, D. H. Multifunctional Wearable Devices for Diagnosis and Therapy of Movement Disorders. *Nat. Nanotechnol.* **2014**, *9* (5), 397–404.
- (4) Ma, Z.; Li, H.; Jing, X.; Liu, Y.; Mi, H. Y. Recent Advancements in Self-Healing Composite Elastomers for Flexible Strain Sensors: Materials, Healing Systems, and Features. *Sens. Actuators, A* **2021**, 329, 112800.
- (5) Latif, S.; Amin, S.; Haroon, S. S.; Sajjad, I. A. Self-Healing Materials for Electronic Applications: An Overview. *Mater. Res. Express* **2019**, *6* (6), 062001.
- (6) Yue, H.; Wang, Z.; Zhen, Y. Recent Advances of Self-Healing Electronic Materials Applied in Organic Field-Effect Transistors. *ACS Omega* **2022**, *7* (22), 18197–18205.
- (7) Mashkoor, F.; Lee, S. J.; Yi, H.; Noh, S. M.; Jeong, C. Self-Healing Materials for Electronics Applications. *Int. J. Mol. Sci.* **2022**, 23 (2), 622.
- (8) Laysandra, L.; Njotoprajitno, A.; Prakoso, S. P.; Chiu, Y. C. From Stretchable and Healable to Self-Healing Semiconducting Polymers: Design and Their TFT Devices. *Mater. Adv.* **2022**, *3* (19), 7154–7184.
- (9) Müllen, K.; Pisula, W. Donor-Acceptor Polymers. J. Am. Chem. Soc. 2015, 137 (30), 9503–9505.
- (10) Himmelberger, S.; Salleo, A. Engineering Semiconducting Polymers for Efficient Charge Transport. *MRS Commun.* **2015**, *5* (3), 383–395.

- (11) Nielsen, C. B.; Turbiez, M.; McCulloch, I. Recent Advances in the Development of Semiconducting DPP-Containing Polymers for Transistor Applications. *Adv. Mater.* **2013**, *25* (13), 1859–1880.
- (12) Tsao, H. N.; Müllen, K. Improving Polymer Transistor Performance via Morphology Control. *Chem. Soc. Rev.* **2010**, 39 (7), 2372–2386.
- (13) Noriega, R.; Rivnay, J.; Vandewal, K.; Koch, F. P. V.; Stingelin, N.; Smith, P.; Toney, M. F.; Salleo, A. A General Relationship between Disorder, Aggregation and Charge Transport in Conjugated Polymers. *Nat. Mater.* **2013**, *12* (11), 1038–1044.
- (14) Sirringhaus, H.; Bird, M.; Zhao, N.; Zhao, N. Charge Transport Physics of Conjugated Polymer Field-Effect Transistors. *Adv. Mater.* **2010**, 22 (34), 3893–3898.
- (15) Root, S. E.; Savagatrup, S.; Printz, A. D.; Rodriquez, D.; Lipomi, D. J. Mechanical Properties of Organic Semiconductors for Stretchable, Highly Flexible, and Mechanically Robust Electronics. *Chem. Rev.* **2017**, *117* (9), 6467–6499.
- (16) Liu, D.; Mun, J.; Chen, G.; Schuster, N. J.; Wang, W.; Zheng, Y.; Nikzad, S.; Lai, J. C.; Wu, Y.; Zhong, D.; Lin, Y.; Lei, Y.; Chen, Y.; Gam, S.; Chung, J. W.; Yun, Y.; Tok, J. B. H.; Bao, Z. A Design Strategy for Intrinsically Stretchable High-Performance Polymer Semiconductors: Incorporating Conjugated Rigid Fused-Rings with Bulky Side Groups. *J. Am. Chem. Soc.* 2021, 143 (30), 11679—11689.
- (17) Sugiyama, F.; Kleinschmidt, A. T.; Kayser, L. V.; Rodriquez, D.; Finn, M.; Alkhadra, M. A.; Wan, J. M. H.; Ramírez, J.; Chiang, A. S. C.; Root, S. E.; Savagatrup, S.; Lipomi, D. J. Effects of Flexibility and Branching of Side Chains on the Mechanical Properties of Low-Bandgap Conjugated Polymers. *Polym. Chem.* **2018**, 9 (33), 4354–4363.
- (18) Yen, H.-C.; Lin, Y.-C.; Chen, W.-C. Modulation of the Hydrophilicity on Asymmetric Side Chains of Isoindigo-Based Polymers for Improving Carrier Mobility-Stretchability Properties. *Macromolecules* **2021**, *54*, 1665–1676.
- (19) Zhang, S.; Alesadi, A.; Mason, G. T.; Chen, K. L.; Freychet, G.; Galuska, L.; Cheng, Y. H.; St. Onge, P. B. J.; Ocheje, M. U.; Ma, G.; Qian, Z.; Dhakal, S.; Ahmad, Z.; Wang, C.; Chiu, Y. C.; Rondeau-Gagné, S.; Xia, W.; Gu, X. Molecular Origin of Strain-Induced Chain Alignment in PDPP-Based Semiconducting Polymeric Thin Films. Adv. Funct. Mater. 2021, 31, 2100161.
- (20) Chiang, Y. C.; Wu, H. C.; Wen, H. F.; Hung, C. C.; Hong, C. W.; Kuo, C. C.; Higashihara, T.; Chen, W. C. Tailoring Carbosilane Side Chains toward Intrinsically Stretchable Semiconducting Polymers. *Macromolecules* **2019**, 52 (11), 4396–4404.
- (21) Mun, J.; Wang, G. J. N.; Oh, J. Y.; Katsumata, T.; Lee, F. L.; Kang, J.; Wu, H. C.; Lissel, F.; Rondeau-Gagné, S.; Tok, J. B. H.; Bao, Z. Effect of Nonconjugated Spacers on Mechanical Properties of Semiconducting Polymers for Stretchable Transistors. *Adv. Funct. Mater.* **2018**, 28 (43), 1804222.
- (22) Savagatrup, S.; Zhao, X.; Chan, E.; Mei, J.; Lipomi, D. J. Effect of Broken Conjugation on the Stretchability of Semiconducting Polymers. *Macromol. Rapid Commun.* **2016**, *37* (19), 1623–1628.
- (23) Oh, J. Y.; Rondeau-Gagné, S.; Chiu, Y. C.; Chortos, A.; Lissel, F.; Wang, G. J. N.; Schroeder, B. C.; Kurosawa, T.; Lopez, J.; Katsumata, T.; Xu, J.; Zhu, C.; Gu, X.; Bae, W. G.; Kim, Y.; Jin, L.; Chung, J. W.; Tok, J. B. H.; Bao, Z. Intrinsically Stretchable and Healable Semiconducting Polymer for Organic Transistors. *Nature* 2016, 539 (7629), 411–415.
- (24) Zheng, Y.; Ashizawa, M.; Zhang, S.; Kang, J.; Nikzad, S.; Yu, Z.; Ochiai, Y.; Wu, H. C.; Tran, H.; Mun, J.; Zheng, Y. Q.; Tok, J. B. H.; Gu, X.; Bao, Z. Tuning the Mechanical Properties of a Polymer Semiconductor by Modulating Hydrogen Bonding Interactions. *Chem. Mater.* **2020**, 32 (13), 5700–5714.
- (25) Zhao, Y.; Zhao, X.; Zang, Y.; Di, C. A.; Diao, Y.; Mei, J. Conjugation-Break Spacers in Semiconducting Polymers: Impact on Polymer Processability and Charge Transport Properties. *Macromolecules* **2015**, *48* (7), 2048–2053.
- (26) Zhao, X.; Zhao, Y.; Ge, Q.; Butrouna, K.; Diao, Y.; Graham, K. R.; Mei, J. Complementary Semiconducting Polymer Blends: The

- Influence of Conjugation-Break Spacer Length in Matrix Polymers. *Macromolecules* **2016**, 49 (7), 2601–2608.
- (27) Zhao, Y.; Zhao, X.; Roders, M.; Gumyusenge, A.; Ayzner, A. L.; Mei, J. Melt-Processing of Complementary Semiconducting Polymer Blends for High Performance Organic Transistors. *Adv. Mater.* **2017**, 29 (6), 1605056.
- (28) Müller, C.; Goffri, S.; Breiby, D. W.; Andreasen, J. W.; Chanzy, H. D.; Janssen, R. A. J.; Nielsen, M. M.; Radano, C. P.; Sirringhaus, H.; Smith, P.; Stingelin-Stutzmann, N. Tough, Semiconducting Polyethylene-Poly(3-Hexylthiophene) Diblock Copolymers. *Adv. Funct. Mater.* **2007**, *17* (15), 2674–2679.
- (29) Ditte, K.; Perez, J.; Chae, S.; Hambsch, M.; Al-Hussein, M.; Komber, H.; Formanek, P.; Mannsfeld, S. C. B.; Fery, A.; Kiriy, A.; Lissel, F. Ultrasoft and High-Mobility Block Copolymers for Skin-Compatible Electronics. *Adv. Mater.* **2021**, 33 (4), 2005416.
- (30) Zhang, S.; Ocheje, M. U.; Huang, L.; Galuska, L.; Cao, Z.; Luo, S.; Cheng, Y.; Ehlenberg, D.; Goodman, R. B.; Zhou, D.; Liu, Y.; Chiu, Y.; Azoulay, J. D.; Rondeau-Gagné, S.; Gu, X. The Critical Role of Electron-Donating Thiophene Groups on the Mechanical and Thermal Properties of Donor-Acceptor Semiconducting Polymers. *Adv. Electron. Mater.* **2019**, *5* (5), 1800899.
- (31) Sato, K.; Hemmi, Y.; Kato, A.; Matsui, H.; Fuchise, K.; Higashihara, T. Precise Synthesis of  $\alpha,\omega$ -Chain-End-Functionalized Poly(Dimethylsiloxane) with Bromoaryl Groups for Incorporation in Naphthalene-Diimide-Based N-Type Semiconducting Polymers. *Polymer* **2022**, 252, 124934.
- (32) Peng, R.; Pang, B.; Hu, D.; Chen, M.; Zhang, G.; Wang, X.; Lu, H.; Cho, K.; Qiu, L. An ABA Triblock Copolymer Strategy for Intrinsically Stretchable Semiconductors. *J. Mater. Chem. C* **2015**, 3 (15), 3599–3606.
- (33) Hsu, L. C.; Kobayashi, S.; Isono, T.; Chiang, Y. C.; Ree, B. J.; Satoh, T.; Chen, W. C. Highly Stretchable Semiconducting Polymers for Field-Effect Transistors through Branched Soft-Hard-Soft Type Triblock Copolymers. *Macromolecules* **2020**, *53* (17), 7496–7510.
- (34) Liu, D.; Ding, Z.; Wu, Y.; Liu, S. F.; Han, Y.; Zhao, K. In Situ Study of Molecular Aggregation in Conjugated Polymer/Elastomer Blends toward Stretchable Electronics. *Macromolecules* **2022**, *55* (1), 297–308.
- (35) Chiang, Y. C.; Shih, C. C.; Tung, S. H.; Chen, W. C. Blends of Polythiophene Nanowire/Fluorine Rubber with Multiscale Phase Separation Suitable for Stretchable Semiconductors. *Polymer* **2018**, *155* (May), 146–151.
- (36) Kulatunga, P.; Yousefi, N.; Rondeau-Gagné, S. Polyethylene and Semiconducting Polymer Blends for the Fabrication of Organic Field-Effect Transistors: Balancing Charge Transport and Stretchability. *Chemosensors* **2022**, *10* (6), 201.
- (37) Shin, M.; Oh, J. Y.; Byun, K. E.; Lee, Y. J.; Kim, B.; Baik, H. K.; Park, J. J.; Jeong, U. Polythiophene Nanofibril Bundles Surface-Embedded in Elastomer: A Route to a Highly Stretchable Active Channel Layer. *Adv. Mater.* **2015**, *27* (7), 1255–1261.
- (38) Xu, J.; Wang, S.; Wang, G. J. N.; Zhu, C.; Luo, S.; Jin, L.; Gu, X.; Chen, S.; Feig, V. R.; To, J. W. F.; Rondeau-Gagné, S.; Park, J.; Schroeder, B. C.; Lu, C.; Oh, J. Y.; Wang, Y.; Kim, Y. H.; Yan, H.; Sinclair, R.; Zhou, D.; Xue, G.; Murmann, B.; Linder, C.; Cai, W.; Tok, J. B. H.; Chung, J. W.; Bao, Z. Highly Stretchable Polymer Semiconductor Films through the Nanoconfinement Effect. *Science* 2017, 355 (6320), 59–64.
- (39) Janasz, L.; Borkowski, M.; Blom, P. W. M.; Marszalek, T.; Pisula, W. Organic Semiconductor/Insulator Blends for Elastic Field-Effect Transistors and Sensors. *Adv. Funct. Mater.* **2022**, 32 (7), 2105456.
- (40) Riera-Galindo, S.; Leonardi, F.; Pfattner, R.; Mas-Torrent, M. Organic Semiconductor/Polymer Blend Films for Organic Field-Effect Transistors. *Adv. Mater. Technol.* **2019**, 4 (9), 1900104.
- (41) Tran, H.; Feig, V. R.; Liu, K.; Wu, H. C.; Chen, R.; Xu, J.; Deisseroth, K.; Bao, Z. Stretchable and Fully Degradable Semiconductors for Transient Electronics. *ACS Cent. Sci.* **2019**, 5 (11), 1884–1891.

- (42) Choi, D.; Kim, H.; Persson, N.; Chu, P. H.; Chang, M.; Kang, J. H.; Graham, S.; Reichmanis, E. Elastomer-Polymer Semiconductor Blends for High-Performance Stretchable Charge Transport Networks. *Chem. Mater.* **2016**, 28 (4), 1196–1204.
- (43) Wang, Y.; Chen, K. L.; Prine, N.; Rondeau-Gagné, S.; Chiu, Y. C.; Gu, X. Stretchable and Self-Healable Semiconductive Composites Based on Hydrogen BondingCross-Linked Elastomeric Matrix. *Adv. Funct. Mater.* **2023**, *33*, 2303031.
- (44) Zhang, G.; Lee, S.; Gutiérrez-Meza, E.; Buckley, C.; McBride, M.; Valverde-Chávez, D. A.; Kwon, Y. H.; Savikhin, V.; Xiong, H.; Dunn, T. J.; Toney, M. F.; Yuan, Z.; Silva, C.; Reichmanis, E. Robust and Stretchable Polymer Semiconducting Networks: From Film Microstructure to Macroscopic Device Performance. *Chem. Mater.* 2019, 31 (17), 6530–6539.
- (45) Song, E.; Kang, B.; Choi, H. H.; Sin, D. H.; Lee, H.; Lee, W. H.; Cho, K. Stretchable and Transparent Organic Semiconducting Thin Film with Conjugated Polymer Nanowires Embedded in an Elastomeric Matrix. *Adv. Electron. Mater.* **2016**, *2*, 1500250.
- (46) Zhang, G.; McBride, M.; Persson, N.; Lee, S.; Dunn, T. J.; Toney, M. F.; Yuan, Z.; Kwon, Y. H.; Chu, P. H.; Risteen, B.; Reichmanis, E. Versatile Interpenetrating Polymer Network Approach to Robust Stretchable Electronic Devices. *Chem. Mater.* **2017**, 29 (18), 7645–7652.
- (47) Nikzad, S.; Wu, H. C.; Kim, J.; Mahoney, C. M.; Matthews, J. R.; Niu, W.; Li, Y.; Wang, H.; Chen, W. C.; Toney, M. F.; He, M.; Bao, Z. Inducing Molecular Aggregation of Polymer Semiconductors in a Secondary Insulating Polymer Matrix to Enhance Charge Transport. *Chem. Mater.* 2020, 32 (2), 897–905.
- (48) Jeong, Y. J.; Jung, J.; Suh, E. H.; Yun, D. J.; Oh, J. G.; Jang, J. Self-Healable and Stretchable Organic Thermoelectric Materials: Electrically Percolated Polymer Nanowires Embedded in Thermoplastic Elastomer Matrix. *Adv. Funct. Mater.* **2020**, *30* (9), 1905809.
- (49) Zhang, S.; Cheng, Y.; Galuska, L.; Roy, A.; Lorenz, M.; Chen, B.; Luo, S.; Li, Y.; Hung, C.; Qian, Z.; St. Onge, P. B. J.; Mason, G. T.; Cowen, L.; Zhou, D.; Nazarenko, S. I.; Storey, R. F.; Schroeder, B. C.; Rondeau-Gagné, S.; Chiu, Y.; Gu, X. Tacky Elastomers to Enable Tear-Resistant and Autonomous Self-Healing Semiconductor Composites. *Adv. Funct. Mater.* **2020**, *30* (27), 2000663.
- (50) Zheng, Y.; Yu, Z.; Zhang, S.; Kong, X.; Michaels, W.; Wang, W.; Chen, G.; Liu, D.; Lai, J. C.; Prine, N.; Zhang, W.; Nikzad, S.; Cooper, C. B.; Zhong, D.; Mun, J.; Zhang, Z.; Kang, J.; Tok, J. B. H.; McCulloch, I.; Qin, J.; Gu, X.; Bao, Z. A Molecular Design Approach towards Elastic and Multifunctional Polymer Electronics. *Nat. Commun.* 2021, 12 (1), 5701.
- (51) Li, N.; Li, Y.; Cheng, Z.; Liu, Y.; Dai, Y.; Kang, S.; Li, S.; Shan, N.; Wai, S.; Ziaja, A.; Wang, Y.; Strzalka, J.; Liu, W.; Zhang, C.; Gu, X.; Hubbell, J. A.; Tian, B.; Wang, S. Bioadhesive Polymer Semiconductors and Transistors for Intimate Biointerfaces. *Science* 2023, 381 (6658), 686–693.
- (52) Angunawela, I.; Nahid, M. M.; Ghasemi, M.; Amassian, A.; Ade, H.; Gadisa, A. The Critical Role of Materials' Interaction in Realizing Organic Field-Effect Transistors Via High-Dilution Blending with Insulating Polymers. ACS Appl. Mater. Interfaces 2020, 12 (23), 26239–26249.
- (53) Sekitani, T.; Zschieschang, U.; Klauk, H.; Someya, T. Flexible Organic Transistors and Circuits with Extreme Bending Stability. *Nat. Mater.* **2010**, *9* (12), 1015–1022.
- (54) Yu, K.; Park, B.; Kim, G.; Kim, C. H.; Park, S.; Kim, J.; Jung, S.; Jeong, S.; Kwon, S.; Kang, H.; Kim, J.; Yoon, M. H.; Lee, K. Optically Transparent Semiconducting Polymer Nanonetwork for Flexible and Transparent Electronics. *Proc. Natl. Acad. Sci. U.S.A.* **2016**, *113* (50), 14261–14266.
- (55) Wang, S.; Fabiano, S.; Himmelberger, S.; Puzinas, S.; Crispin, X.; Salleo, A.; Berggren, M. Experimental Evidence That Short-Range Intermolecular Aggregation Is Sufficient for Efficient Charge Transport in Conjugated Polymers. *Proc. Natl. Acad. Sci. U.S.A.* **2015**, *112* (34), 10599–10604.

- (56) Bhaumik, S.; Ntetsikas, K.; Hadjichristidis, N. Noncovalent Supramolecular Diblock Copolymers: Synthesis and Microphase Separation. *Macromolecules* **2020**, 53 (15), 6682–6689.
- (57) Chen, S.; Binder, W. H. Dynamic Ordering and Phase Segregation in Hydrogen-Bonded Polymers. *Acc. Chem. Res.* **2016**, 49 (7), 1409–1420.
- (58) Stuparu, M. C.; Khan, A.; Hawker, C. J. Phase Separation of Supramolecular and Dynamic Block Copolymers. *Polym. Chem.* **2012**, 3 (11), 3033–3044.
- (59) Rao, J.; Păunescu, E.; Mirmohades, M.; Gadwal, I.; Khaydarov, A.; Hawker, C. J.; Bang, J.; Khan, A. Supramolecular Mimics of Phase Separating Covalent Diblock Copolymers. *Polym. Chem.* **2012**, 3 (8), 2050–2056.
- (60) Lin, Y. H.; Darling, S. B.; Nikiforov, M. P.; Strzalka, J.; Verduzco, R. Supramolecular Conjugated Block Copolymers. *Macromolecules* **2012**, *45* (16), 6571–6579.
- (61) Yan, X.; Liu, Z.; Zhang, Q.; Lopez, J.; Wang, H.; Wu, H. C.; Niu, S.; Yan, H.; Wang, S.; Lei, T.; Li, J.; Qi, D.; Huang, P.; Huang, J.; Zhang, Y.; Wang, Y.; Li, G.; Tok, J. B. H.; Chen, X.; Bao, Z. Quadruple H-Bonding Cross-Linked Supramolecular Polymeric Materials as Substrates for Stretchable, Antitearing, and Self-Healable Thin Film Electrodes. J. Am. Chem. Soc. 2018, 140 (15), 5280–5289.
- (62) Chen, Y.; Kushner, A. M.; Williams, G. A.; Guan, Z. Multiphase Design of Autonomic Self-Healing Thermoplastic Elastomers. *Nat. Chem.* **2012**, *4* (6), 467–472.
- (63) Galuska, L. A.; Ocheje, M. U.; Ahmad, Z. C.; Rondeau-Gagné, S.; Gu, X. Elucidating the Role of Hydrogen Bonds for Improved Mechanical Properties in a High-Performance Semiconducting Polymer. *Chem. Mater.* **2022**, 34 (5), 2259–2267.
- (64) Ocheje, M. U.; Charron, B. P.; Cheng, Y. H.; Chuang, C. H.; Soldera, A.; Chiu, Y. C.; Rondeau-Gagné, S. Amide-Containing Alkyl Chains in Conjugated Polymers: Effect on Self-Assembly and Electronic Properties. *Macromolecules* **2018**, *51* (4), 1336–1344.
- (65) Zhang, S.; Galuska, L. A.; Gu, X. Water-Assisted Mechanical Testing of Polymeric Thin-Films. *J. Polym. Sci.* **2022**, *60* (7), 1108–1129.
- (66) Zhang, S.; Ocheje, M. U.; Luo, S.; Ehlenberg, D.; Appleby, B.; Weller, D.; Zhou, D.; Rondeau-Gagné, S.; Gu, X. Probing the Viscoelastic Property of Pseudo Free-Standing Conjugated Polymeric Thin Films. *Macromol. Rapid Commun.* **2018**, 39 (14), 1800092.